RESOURCE GEOLOGY, vol. 56, no. 2, 141–156, 2006

Polymetallic and Au-Ag Mineralizations at the Mutnovskoe Deposit in South Kamchatka, Russia

Ryohei TAKAHASHI, Hiroharu MATSUEDA*, Victor M. OKRUGIN** and Shuji ONO***

Graduate School of Science, Hokkaido University, Kita-ku, N10 W9, Sapporo 060-0810, Japan
[e-mail: ryohei@ep.sci.hokudai.ac.jp]
* *The Hokkaido University Museum, Hokkaido University, Kita-ku, N10 W8, Sapporo 060-0810, Japan*
** *Institute of Volcanology and Seismology FED Academy of Science Russian Federation, 9st Piip, 683006 Petropavlovsk-Kamchatsky, Russia*
*** *Graduate School of Engineering, Hokkaido University, Kita-ku, N13 W8, Sapporo 060-8628, Japan*
Received on March 9, 2005; accepted on February 14, 2006

Abstract: The Mutnovskoe deposit located in the Porozhisto-Asachinskaya metallogenic province of South Kamchatka, Russia, is a polymetallic vein and Au-Ag quartz vein associated type of hydrothermal deposit. The Mutnovskoe deposit is located inside a paleo-caldera structure at the center of the Mutnovsko-Asachinskaya geothermal field of Pliocene - Quaternary age, where active gold deposition is identified in hot spring precipitate.

The Mutnovskoe deposit is subdivided into the north flank, the central flank and the south flank based on the vein distributions and mineral parageneses. The mineralized vein system is oriented N-S hosted in diorite - gabbroic diorite stock, volcanic rocks and sedimentary rocks of Miocene - Pleistocene age. The mineralization stage I (polymetallic vein) mainly in the central and the south flanks is Zn-Pb-Cu-Au-Ag contained in sphalerite, galena and tetrahedrite-tennantite group mineral. The stage II (Au-Ag quartz vein) occurs in the north and the central flanks. The stage III (Mn-sulfide and Mn-Ca-carbonate vein) occurs in the whole deposit area. Stage II is the typical Au-Ag quartz-adularia vein of low-sulfidation type. Stage III is alabandite-rhodochrosite-quartz-calcite vein. The K-Ar ages are 1.3±0.1 Ma for stage I sericite in alteration zone, and 0.7±0.1 Ma for the stage II adularia in mineralized vein.

Based on the fluid inclusion study, range of ore forming temperature of the Mutnovskoe deposit is 200 to 260˚C (av. 230˚C). Salinities of fluid inclusions indicate 2.2 to 5.7 wt% NaCl in sphalerite and 0.8 to 3.3 wt% NaCl in quartz for the stage I.

Mineral paragenesis of the polymetallic vein (stage I) is characterized by a district zoning of tennantite and Cd-rich sphalerite in the south flank and tetrahedrite and Mn-rich sphalerite in the central flank, which is due to the fractional crystallizations of ore-forming fluid. Depositional condition of the low sulfidation state is inferred for the Mutnovskoe deposit, where the polymetallic vein of the south flank is in relatively higher sulfidation state than the central flank.

Keywords: hydrothermal mineralization, K-Ar age, fluid inclusion, physicochemical condition, sulfidation state, Mutnovskoe, Kamchatka, Russia

1. Introduction

The potential of metallogenic resources in Kamchatka peninsula is being remarked by recent explorations (Liessman and Okrugin, 1994; Patoka et al., 1998; MITI, 2001), however, there have been only a few academic researches detailing each deposit because of political constrains and the wilderness character of this region. During the Soviet Union era, admittance to the Kamchatka Peninsula for international and even domestic scientists had been restricted until 1992 mainly due to political affairs. The Kamchatka Peninsula has a land area of 472,300 km^2 being 1.3 times larger than the Japan islands, and a population of about three hundred-thousand persons. The climate and geography are cool monsoon and mountainous with permafrost and glacier at higher altitude.

The Mutnovsko-Asachinskaya geothermal area including the Mutnovskoe deposit is known to be of high potential for geothermal energy; two geothermal power-plants are operative. Many natural hot springs are observed around the active volcano of Mt. Mutnovsky (Fig. 1). Many epithermal deposits of mainly Au-Ag vein and minor Cu-Pb-Zn vein are located in the Porozhisto-Asachinskaya metallogenic province of South Kamchatka within the geothermal area, for example, the Vilyuchinskoe Au deposit and Rodnikovoe Au deposit of 1.1-0.9± 0.1Ma (Takahashi et al., 2002) in the north, the Mutnovskoe Au-Ag-Cu-Pb-Zn deposit in the central, and the Asachinskoe Au deposit of 4.5±0.1 Ma (Takahashi et al., 2001) in the south (Fig. 1). Reportedly, AngloGold Ashanti Ltd. (AGA) of the USA, Trans Siberian Gold Ltd. (TSG) of the UK and Trevozhnoye Zarevo Ltd. (TZ) of the Russia have started mining operation at the Asachinskoe deposit from 2005, and is also proceeding the scooping study required for mining the Rodnikovoe deposit

(e.g., Nally, 2003; Trans-Siberian Gold PLC, 2004).

The Mutnovskoe deposit has been known formerly as a complex type of mineralizations of "Au-Ag quartz vein" and "Pb-Zn sulfide vein" distributed in wide area of 10 km^2. Geological description have been carried out since 1970's (Vasilevsky et al., 1977a), and the most of tributary rivers of R. Mutnovskaya and local zones in the Mutnovskoe deposit were named during the geological survey. The total ore reserves are estimated to be 23.5 t Au, 1,384 t Ag, 100,000 t Pb and 100,000 t Zn on the basis of the prospect of about 20 drill-holes of ca. 10,000 m in total length and numerous trenches during 1975–1981 (Patoka et al., 1998; Okrugin, 1995).

The purpose of this study is to clarify ore-forming conditions of the Mutnovskoe deposit on the basis of the characteristics of mineralizations, i.e., K-Ar ages, mineralogy, fluid inclusions and physicochemical calculation. This will provide the contextual data for the mining development of epithermal deposits in the Mutnovskaya area for future.

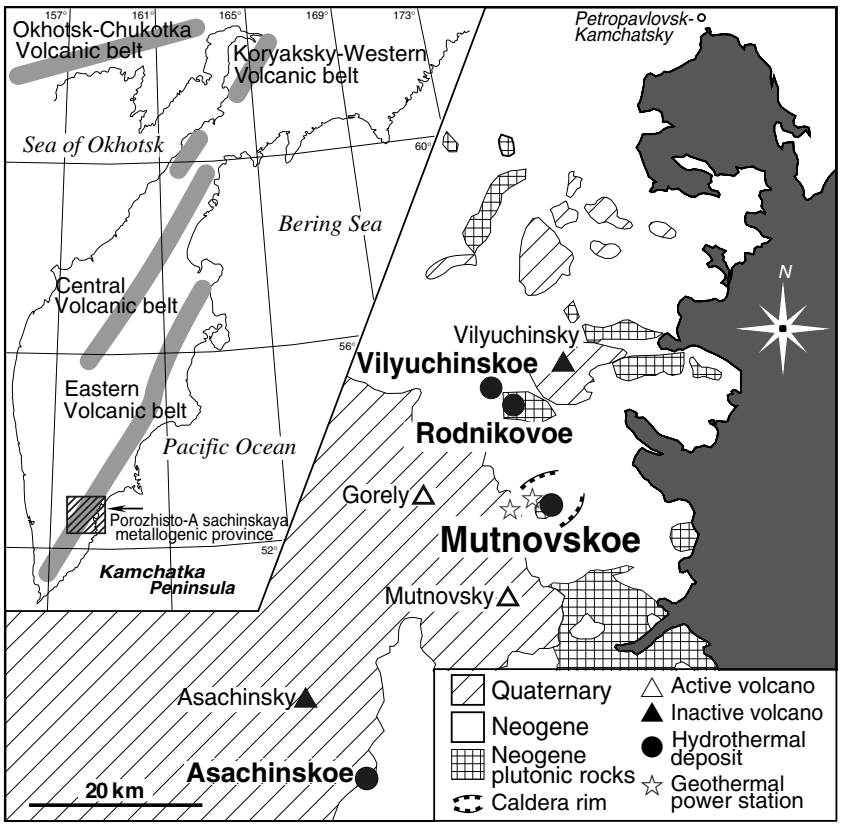

Fig. 1 Simplified geological map in the Porozhisto-Asachinskaya metallogenic province of South Kamchatka. Distribution of four volcanic belts is shown as gray thick lines in the areas of Eurasia continent and Kamchatka Peninsula.

2. Geological Outline

2.1. Geology of the surrounding area

The Kamchatka Peninsula consists of the Koryaksky-Western, the Central and the Eastern Volcanic Belts with NNE-SSW trending stepwise distribution (Fig. 1). These three volcanisms (Paleocene - recent) are subsequent to the Okhotsk - Chukotka volcanism (Cretaceous - Paleocene) in the eastern margin of Eurasia continent (Zonenshain et al., 1990). The present volcanism is observed in the Eastern Kamchatka Volcanic Belt including South Kamchatka area (Masurenkov, 1991; Fedotov, 1991). The Eastern Kamchatka volcanism is due to the arc-trench system of the Circum-Pacific belt. The Mutnovsko-Asachinskaya geothermal area in South Kamchatka, located 50-80 km south of Petropavlovsk-Kamchatsky city (Fig. 1), is highly potential for hydrothermal activity (e.g., Vasilevsky et al., 1977a, 1977b; Okrugin et al., 1994a; Okrugin, 1995; Petrenko and Bolshakov, 1995; Petrenko, 1998a, 1999; Leonov, 2000). The area consists chiefly of Tertiary and Quaternary volcanic rocks. Petrenko (1998a) reported that the volcanic rocks in South Kamchatka formed in three stages: Oligocene to Miocene (andesite), Late Miocene to Pliocene (basalt, andesite and rhyolite) and Quaternary (basalt and andesite). Sedimentary and volcanic rocks of Oligocene to Miocene are exposed along the east coast. Intrusive rocks related to the volcanism are plutons and dikes of gabbro, diorite, and andesite composition of Miocene to Pliocene age (e.g., Petrenko, 1998a, 1999; Ministry of International Trade and Industry, abbreviated hereafter to MITI, 2001). The gabbro and diorite show high magnetic susceptibility (50–60×10^{-3} S.I.) characteristics of magnetite series granitoids. According to Kirsanov and Melekestsev (1991), formation of the Mutnovsky volcano (2,323 m) had started in the Late Pleistocene, and the latest phreatic eruption occurred in March, 2000 (Okrugin et al., 2001). A tephrochronological study (Melekestsev et al., 1987) shows that formation of the Gorely volcano (1,829 m) started in the Early Pleistocene, resulting in the formation of four crater lakes. Ignimbrite (consisted of welded tuff and pumice) surged from the Gorely volcano now covers an area of approximately 600 km^2. The thickness of the ignimbrite deposit ranges from 5 to 30 m on the flank of the Gorely volcano,

and from 300 to 350 m on the periphery of 15–20 km far from the volcanic center (Melekestsev et al., 1987).

2.2. Geology of the Mutnovskoe deposit

The Mutnovskoe deposit is Au-Ag quartz vein and polymetallic vein associated type of deposit. The deposit is located in the upstream part of the Mutnovskaya River and its tributaries of Zheltyi, Rudnyi and Avgustovskaya carving deep canyons. The Mutnovskoe deposit is situated at the junction of South Kamchatka fault (N-S system) and Mutnovsk fault (NE-SW), within an eroded caldera of Pliocene-Lower Pleistocene age (Fig. 2). There are more than 160 veins in 10 km^2 wide area (MITI, 2001). The deposit area is surrounded by the ridge of caldera with an elevation of about 1,100 m. The oldest outcropping rocks are marine arenaceous shale of Lower Miocene age based on the identification of marine fauna (Vlasov, 1967). This shale is overlain by Lower-Middle Miocene submarine basaltic - andesitic lava and tuffs, occurring in the eastern part of the deposit (e.g., Sheimovich and Karpenko, 1996). The Miocene-Pleistocene (?) subvolcanic diorite - gabbroic diorite stock is exposed in the center of the deposit (Fig. 2), and is correlated with the Zhirovsky paleovolcano complex developed between the Upper Pliocene and the Pleistocene (?) (Lattanzi et al., 1995; Sheimovich and Karpenko, 1996). The diorite - gabbroic diorite consists of medium to coarse-grained phenocrysts of plagioclase, hornblende and quartz, which is similar to the diorite-gabbroic diorite complex at the Rodnikovoe deposit. Formerly the gabbroic diorite is considered to be Miocene-Pliocene age based on the geological structure (Vasilevsky et al., 1977a). The diorite-gabbroic diorite is thought to be unconformably overlain by Pliocene tuff and Pleistocene volcanics (dacite, rhyolite, dacitic and rhyolitic tuff) based on the geological structure and identification of flora. Sheimovich and Karpenko (1996) reported radiometric ages from 0.80±0.04 to 0.63±0.03 Ma for the Pleistocene volcanics. Northwestern part of the deposit is covered by Holocene volcanics, mainly of pyroclastic rock.

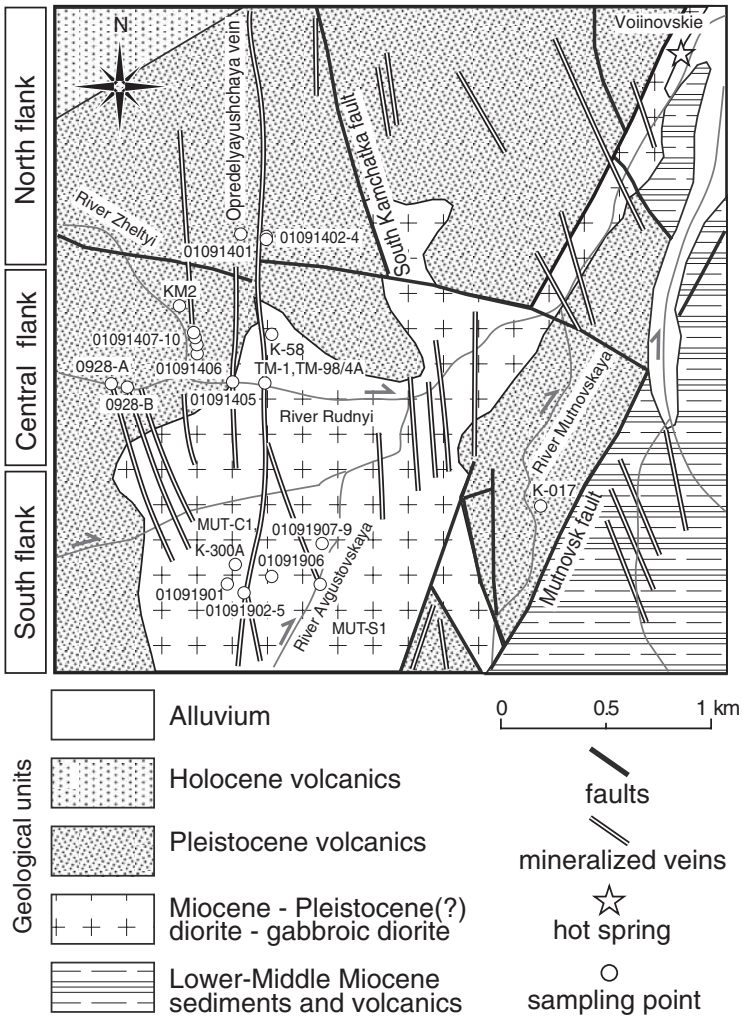

Fig. 2 Geologic map of the Mutnovskoe deposit (after Lattanzi et al., 1995).

The Mutnovskoe deposit area is divided into the north flank and the south flank by their different mineralization characteristics. Between the north and the south flanks, the area around River Rudnyi is designated as the central flank (Fig. 2). An idiomatic usage of "flank" for the areal designation is acceded to the previous reports (e.g. Okrugin, 1995; Patoka et al., 1998). Cu-Pb-Zn polymetallic veins occur in both the central and south flanks, but Au-Ag quartz veins occur in the north and central flanks. Mn-sulfide and Mn-Ca-carbonate-quartz veins occur in the whole deposit, accompanying abundant supergene Mn-oxide. Most mineralized veins are hosted in fractures of N-S system of the gabbroic diorite and the Pleistocene volcanics. For example, a main vein named Opredelyayushchaya vein with N-S trend is recognized to be up to 3.2 km in length, up to 400 m in depth by the drilling survey, which diverges in the central and the south flanks. An outcrop of ore mineralization with 5.5 m width as the diverged Opredelyayushchaya vein is observed along River Rudnyi in the central flank (e.g. sampling points of TM-1 and TM-98/4A in Fig. 2).

In the north flank of Mutnovskoe deposit, the average ore grade is 10.3 g/t Au and 119.7 g/t Ag, suggesting total reserves of 11.5 t Au and 133.8 t Ag. In the south flank, the average ore grade is 2.4 g/t Au, 250 g/t Ag, 2 % of Zn and Pb for more than 5 Mt polymetallic ore (Petrenko, 1998b; Patoka et al., 1998; MITI, 2001). Estimated total

Table 1 Sample description and chemical composition for the Mutnovskoe deposit. Some data of grade analysis is cited after MITI (2001).

	Samples	Type of rocks	Stage	Grade of ores							
				Au (ppb)	Ag (ppm)	As (ppm)	Sb (ppm)	Hg (ppb)	Cu (ppm)	Pb (ppm)	Zn (ppm)
North flank	01091401	Altered dacite with K-felspar and sericite-smectite mixed layer	-	221	3	108	15	1160	30	1	11
	01091402	Quartz vein with vuggy parts	II	1250	31	47	45	1250	78	44	24
	01091403	Quartz vein with massive-flinty structure	II	1980	10	147	50	990	56	18	23
	01091404	Quartz vein with polymetallic sulfide dissemination	II	1670	57	221	57	590	71	150	99
Central flank	01091405	Diorite with weakly propylitic alteration	-								
	01091406	Quartz-carbonate-sulfide vein coated by Mn oxide	I, III	148	14	50	45	110	101	440	3340
	01091407	Quartz-carbonate-sulfide vein coated by Mn oxide	II, III	354	45	142	92	130	270	643	864
	01091408A	Mn-carbonate-sulfide vein	III	207	12	20	22	10	181	472	2020
	01091408B	Quartz vein with massive-flinty structure	II	24	3	29	9	40	126	144	1990
	01091409	Mn-carbonate-sulfide vein	III	91	24	41	54	190	176	1960	9290
	01091410	Quartz-Mn-carbonate-sulfide vein	II, III	766	13	4530	112	280	83	103	1610
	KM-2	Altered tuff with sericite	-								
	K-58*	Quartz vein with banding structure	II	456	15	132	25	690	159	354	1190
	0928-A*	Polymetallic sulfide vein	I	1600	765	2290	686	4800	424	137000	112000
	TM-1*	Quartz vein with banding structure	II	NSS	16	19	44	40	118	32	142
	TM98/4A*	Quartz vein with brecciation structure of sulfide	I	5460	595	2050	617	80	6730	21900	198000
South flank	01091901	Altered dacite with alunite	-	161	4	26	19	1000	25	144	80
	01091902	Polymetallic sulfide-quartz vein	I	7110	296	5060	2050	460	6720	1960	137000
	01091903	Polymetallic sulfide-quartz vein	I	5760	114	4970	1040	300	7060	1270	9015
	01091904	Polymetallic sulfide-quartz vein	I	4000	1280	34900	38500	1180	130000	3790	121000
	01091905	Diorite with weakly propylitic alteration	-								
	01091906	Quartz-polymetallic sulfide vein with symmetrical growth structure	I	2230	50	533	120	1540	629	1290	56300
	01091907	Quartz-polymetallic sulfide vein	I								
	01091908	Quartz-polymetallic sulfide vein	I								
	01091909	Quartz-polymetallic sulfide vein with brecciation structure	I	1720	494	953	414	900	1580	127000	298000
	MUT-C1	Quartz-polymetallic sulfide vein	I								
	MUT-S1	Polymetallic sulfide-quartz vein	I								
	K-300A*	Quartz-sulfide vein with brecciation structure	I	17350	689	>10000	>1000	160	39900	2190	40600
	K-017*	Quartz-Mn-sulfide-carbonate vein	III	373	102	324	160	2510	702	4650	19900

* Analysis was carried out by Dowa mining company LTD.
NSS: non-sufficient sample, however, another sample collected in same outcrop of TM-1 shows 2390ppb Au and 3ppm Ag.

reserves are 23.5 t Au, 1,384 t Ag, 100,000 t Pb and 100,000 t Zn in the whole Mutnovskoe deposit. According to the analysis of ores in the present study (Table 1), variation of Pb and Zn contents are 0.0002–0.002 % Pb and 0.0002–0.001 % Zn in the north flank, 0.0003–13.7 % Pb and 0.001–19.8 % Zn in the central flank, and 0.1–12.7 % Pb and 0.9–29.8 % Zn in the south flank (Fig. 3). Gold and silver contents show a range of 1.3–2.0 g/t Au and 10–57 g/t Ag in the north flank, 0.02–5.4 g/t Au and 3–765 g/t Ag in the central flank, and 0.3–17.4 g/t Au and 50–1280 g/t Ag in the south flank (Table 1). Zinc and lead occur as sphalerite and galena, respectively, and silver and copper mainly as tetrahedrite group minerals. Gold occurs as electrum in banding quartz vein, and/or as telluride minerals in polymetallic vein.

Hydrothermal activity observed at present as hot spring activities is utilized in geothermal power stations in the west of the deposit, and a hot spring field named

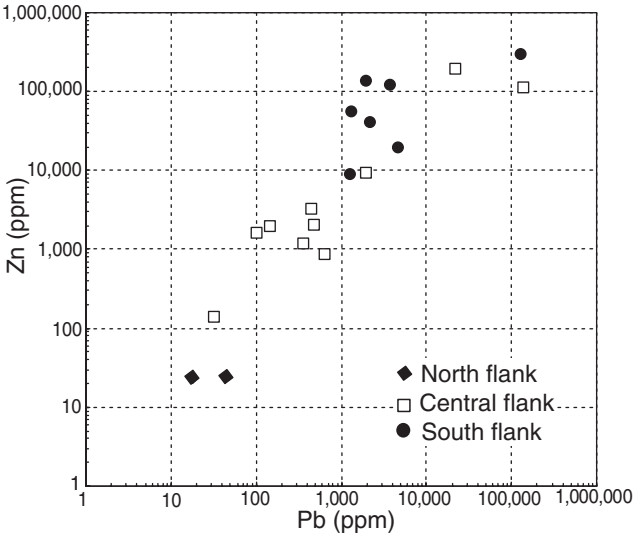

Fig. 3 Diagram of Pb-Zn compositions based on the bulk analysis of ores in the Mutnovskoe deposit.

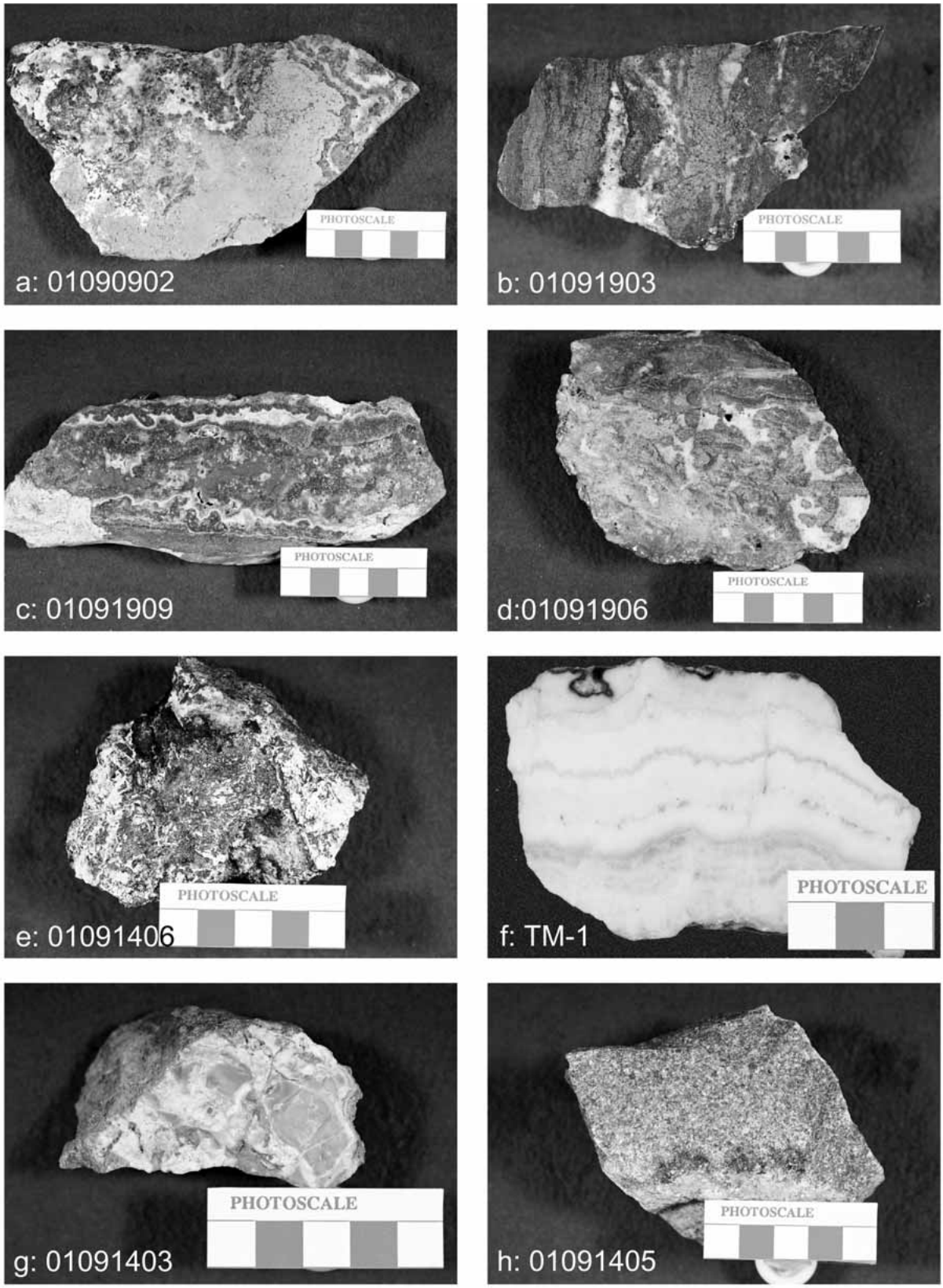

Fig. 4 Samples of the Mutnovskoe deposit. (a – d): Polymetallic vein in the south flank. (e): Quartz-carbonate-sulfides vein in the central flank. (f): Quartz vein in the central flank. (g) Quartz vein in the north flank. (h): Host rock of diorite in the central flank. The scale indicates 1 division = 1 cm.

Table 2 Results of K-Ar dating*.

No.	Deposit sample number	Age	$^{40}Ar/^{40}K$	^{40}Ar ppm	^{40}Ar/Total ^{40}Ar	Ave. ^{40}Ar ppm	K %	Ave. K %	^{40}K ppm	Mineral**	Style of deposits & metal
1	Mutnovskoe Central KM-2	1.3±0.1Ma	0.000075	0.000605 0.000506	0.015 0.043	0.000556	6.296 6.153	6.224	7.426	sericite	polymetalic vein Pb, Zn, Cu, In
2	Mutnovskoe Central K58	0.7±0.1Ma	0.000039	0.000162 0.000191	0.011 0.012	0.000177	3.792 3.784	3.788	4.519	adularia	quartz vein Au, Ag

* The analysis was carried out in Geochron Laboratories, Krueger Enterprises, Inc., U.S.A..
** Major constituent mineral with contamination of quartz.

Voiinovskie is located in north-eastern part of the deposit (Fig. 2). Deposition of sulfides, chiefly melnikovitic pyrite and marcasite including trace gold has been observed in three hot springs (Lattanzi et al., 1995; Okrugin et al., 1994b; Takahashi et al., 2001).

Hydrothermal alteration in the Mutnovskoe deposit was reviewed based on the previous studies and the field observations (e.g. Lattanzi et al., 1995; MITI, 2001). Styles of hydrothermal alteration are classified into the following four types: propylitic (Type I), ore-stage (Type II), hypogene acid-sulfate (Type III) and supergene acid-sulfate (Type IV). A wide area of the Mutnovskoe deposit is characterized by the propylitic alteration (Type I) with pyrite, chlorite, epidote, sericite, calcite and quartz. The ore-stage alteration (Type II) is characterized by quartz, sericite, sericite-smectite mixed layer and ±K-feldspar, occurring in relatively narrow widths of a few meters adjacent to the veins. The acid alterations (Types III-IV) are thought to be in the post ore-stage; the mineral assemblage is pyrite, quartz, kaolinite and ±alunite. Specifically the hypogene acid-sulfate alteration (Type III) forms network clay veins with up to 2 m in width (e.g. sampling point of 01091901 in Fig. 2); the clay vein is not associated with ore mineralization. While the supergene acid-sulfate alteration (Type IV) is characterized by secondary oxidation of pyrite in hydrothermal alteration associated with mineralized vein, and no more than a few decimeters beneath the surface; for example, the alteration is well developed along the banks of the River Zheltyi (e.g. sampling points of KM2 and 01091406-10 in Fig. 2) and near in the confluence of the Rudnyi and the Avgustovskaya Rivers.

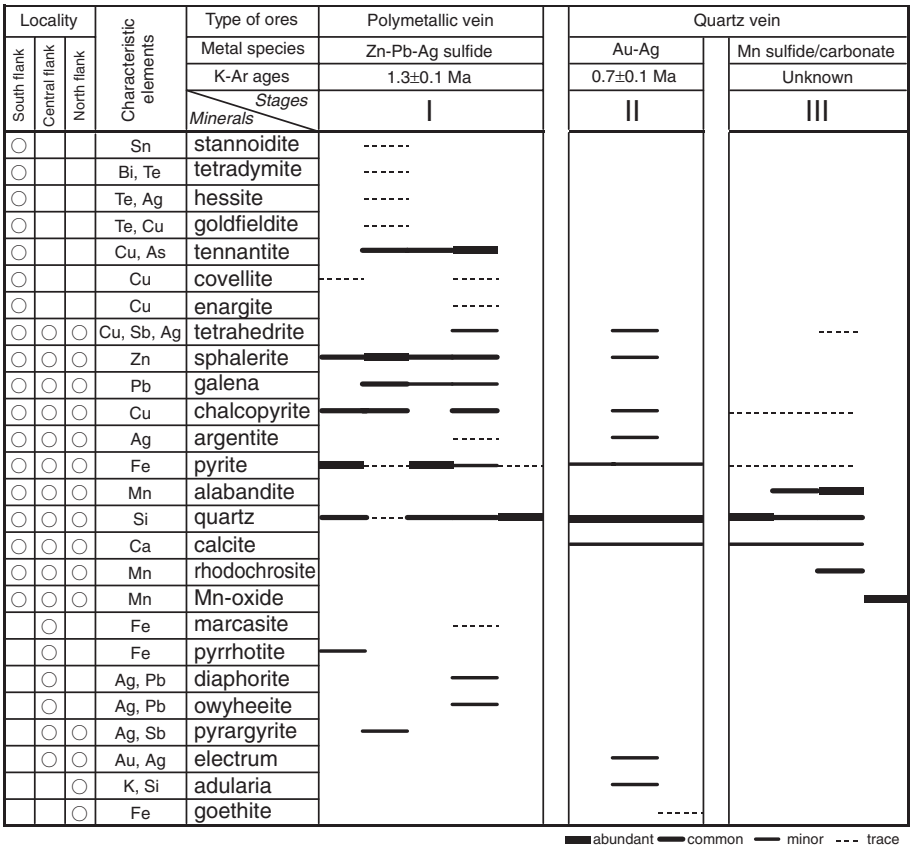

Fig. 5 Mineral paragenesis for the Mutnovskoe deposit.

3. Mineralization Stages

Mineralized veins in the Mutnovskoe deposit are classified by their features into two groups: polymetallic veins (stage I) and quartz veins including Au-Ag-bearing type (stage II) and Mn-bearing type (stage III) (Fig. 5). The polymetallic veins (sulfides 30 - 50 % modal; Fig. 4-a, b, c and d) are distributed mainly in the central and the south flanks of the Mutnovskoe deposit. The quartz veins (sulfides <5 % modal; Fig. 4-f and g) are distributed mainly in the north and the central flanks of the deposit (Lattanzi et al., 1995). The distribution of the polymetallic and quartz veins is overlapped.

Keys to clarify the mineralization stages are (1) mode of occurrence and structure of the ores and (2) K-Ar ages.

(1) The structural association of the polymetallic vein

in the early stage and the Au-Ag quartz vein in the late stage is observed at the main vein of Opredelyayushchaya in the central flank. Cross-cutting structures are observed, in which Au-Ag quartz veins are cut by Mn-sulfide, Mn-Ca-carbonate and quartz associated veins.

(2) K-Ar age of 1.3±0.1 Ma was obtained for mineral concentrate of sericite from the hydrothermal alteration zone adjacent to the polymetallic vein in the central flank (Table 2). The alteration is originated from volcanic tuff, which consists of pure sericite and quartz, and other primary mineral does not remain. K-Ar age of 0.7±0.1 Ma was obtained for mineral concentrate of adularia from the Au-Ag quartz vein in the north flank. The quartz vein shows regularly banding structure of quartz, adularia and sulfide minerals with about 10 cm width based on microscopic observation and K-feldspar dyeing method. Contaminant within the mineral concentrates is quartz based on XRD analysis.

The mineralization stages are stage I (polymetallic vein: Cu-Pb-Zn sulfide mineralization), stage II (quartz vein: Au-Ag mineralization) and stage III (quartz vein: Mn sulfide/carbonate mineralization) on the basis of tectonic boundaries (β-Grenzen) (as defined, e.g. by Kutina, 1955; Nakamura, 1988). Suborder sequences of the mineral paragenesis in each mineralization stage are subdivided for limited ore specimens on the basis of growth boundaries (α-Grenzen) (Fig. 5).

4. Mineralogy

4.1. Analytical method

EPMA chemical analysis was carried out by a JEOL 733 with the measurement conditions as follows; acceleration voltage 15 kV (25 kV for Pb, Bi and Te minerals), beam current 20 nA (15 nA for Pb, Bi and Te minerals), 1-2 μm of probe diameter, and wavelength dispersive spectrometers with TAP, PET and LiF. Standard materials are natural minerals ($CuFeS_2$, PbS, FeAsS and Sb_2S_3), synthesized compounds (ZnS, MnS, SnS, CdS and InP) and pure metals (Ni, Au, Ag, Bi and Te). Data for quantitative analysis were processed by ZAF method.

4.2. Mineralogy

4.2.1. Sphalerite [(Zn, Fe, Cd, Mn, In) S]: Sphalerite is a major ore mineral in the whole Mutnovskoe deposit and was chiefly formed in stages I (Fig. 6-a, b, c, Fig. 7-c and d). The sphalerite often contains fine pyrite inclusions along growth line and chalcopyrite emulsion is also common in stage I. Transparency of the sphalerite increases from early to late sequences (stage I). Coexistence of pyrrhotite and pyrite is observed in the opaque sphalerite from the central flank. The sphalerite occurring in the Au-Ag quartz vein at stage II is commonly fine grained.

FeS contents in the sphalerite are 0.0 - 22.1 mol % for the ores from the central flank, and 0.0 - 2.9 mol % in the south flank of Mutnovskoe (Fig. 8; Table 3). Quantitative analysis of chemical composition of sphalerite shows high manganese contents up to 2.6 atm % in the central flank, and high cadmium contents up to 0.8 atm % for the ores in the south flank of Mutnovskoe (Fig. 9). According to Lattanzi et al. (1995), In-bearing sphalerite with up to 4.7 wt% Cd and 9.3 wt% In occurs in the diverged vein of the Opredelyayushchaya main vein in the south flank.

4.2.2.Tetrahedrite-Tennantite [$(Cu,Ag)_{10}(Fe,Zn)_2Sb_4S_{13}$–$(Cu,Ag)_{10}(Fe,Zn)_2As_4S_{13}$]: Tennantite-tetrahedrite group mineral occurs in early to middle sequence of stage I. At the stage I, the mineral occurs as a massive aggregates (Fig. 6-g), as fine grains of 5 μm to 2 mm coexisting with sphalerite (Fig. 6-b and c), as emulsion texture in galena (Fig. 7-e), and as single mineral with needle shaped texture in quartz (Fig. 6-d). In stage II, tetrahedrite occurs as minor mineral in the Au-Ag quartz vein. EPMA analysis clearly indicates the predominant occurrence of tetrahedrite in the central flank and tennantite-tetrahedrite in the south flank of the deposit throughout the stages I to II (Fig. 10; Table 4). Ag contents of tetrahedrite - tennantite are up to 2.7 atm % for the central flank, and up to 0.5 atm % for the south flank. Goldfieldite (containing Te in solid solution) was found in the south flank (Fig. 6-e).

4.2.3. Galena [PbS]: Galena is a common mineral in the early to middle sequence of stage I, usually associated with sphalerite band with width of several centimeters (Fig. 7-d and e). Exsolutions of tennantite-tetrahedrite and pyrargyrite - proustite solid solutions can be seen commonly in galena at the central flank (Fig. 7-e and f).

4.2.4. Cu-Fe-minerals: Pyrite [FeS_2] occurs abundantly in stages I and II. Marcasite [FeS_2] is observed as trace mineral in the stage I. At early sequence of stage I from the central flank, particularly abundant pyrite has elongated crystal forms (needle shaped texture) of 5 - 10 mm in length, showing weak anisotropy with color of green to orange (Fig. 7-a). Numerous small pores can be seen in single crystal of the needle shaped pyrite, and the pores rim pore-free area. The observed texture of pyrite suggests an origin as pseudomorphs from marcasite inversion by heating (e.g., Murowchick, 1992). Sectional zoning with As concentration is observed in the needle shaped pyrite (Fig. 7-b). EPMA analysis shows As contents of pyrite up to 5.6 wt% in the central flank, while up to 1.1 wt% in the south flank (Fig. 11; Table 5).

Chalcopyrite [$CuFeS_2$] and pyrrhotite [$Fe_{1-x}S$] occur as common and minor minerals in the stage I, respectively. Enargite [$Cu_3(As,Sb)S_4$] fulfills cracks and pores of tennantite secondarily in stage I of the south flank (Fig. 6-g; Table 5). Covellite [CuS] coexists with argentite as mixture in stage I of the south flank (Fig. 6-h; Table 5).

4.2.5. Au-Ag minerals: Usually electrum (10–150 μm in size) with Ag contents of 43.4–56.0 atm % occurs in stage

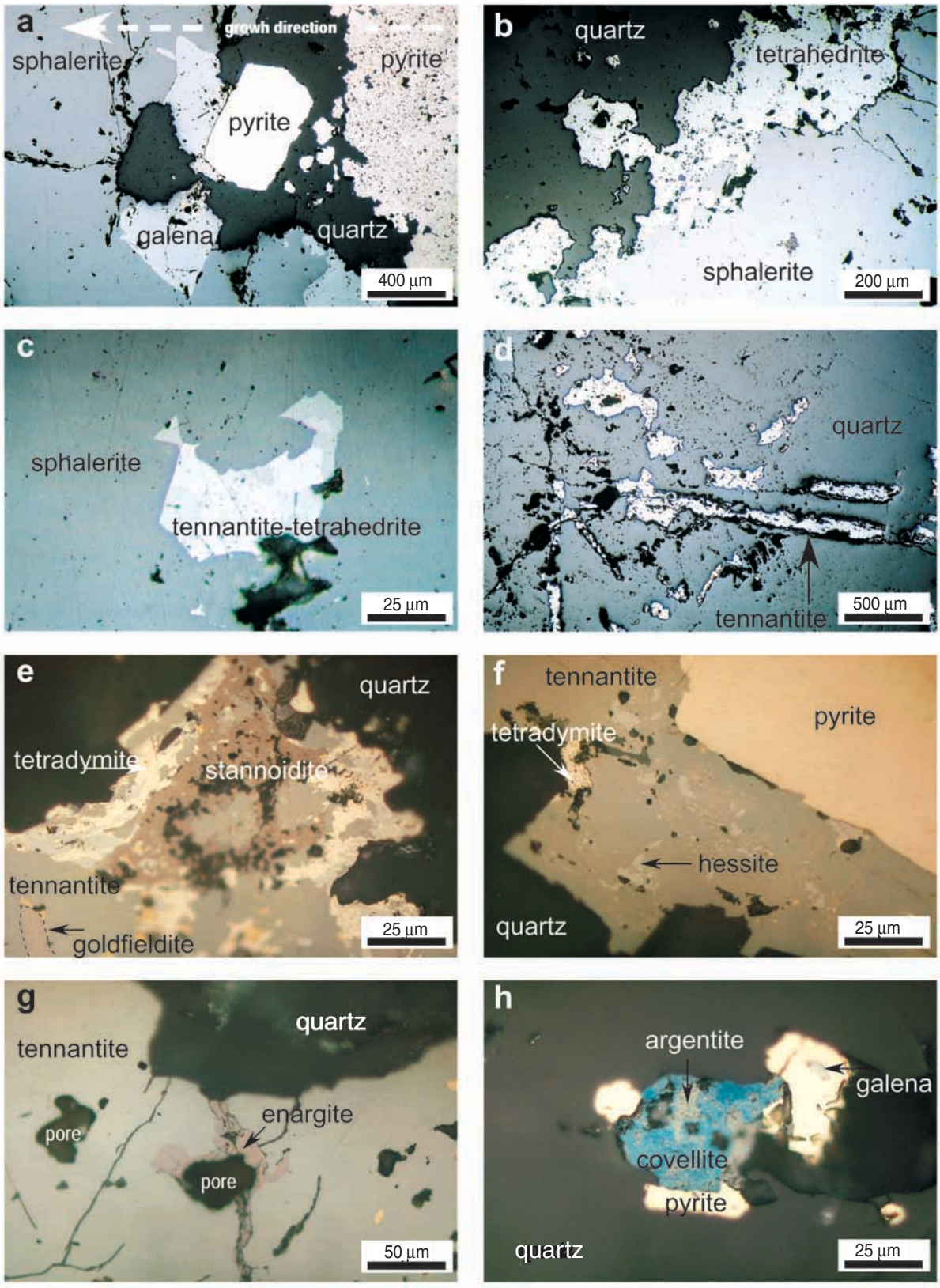

Fig. 6 Photomicrographs of ore minerals in the Mutnovskoe deposit. a: growth boundary of mineralization (01091902), b: In-bearing sphalerite (K-300), c: tennantite with heterogeneous composition (K-300), d: needle shaped tennantite (01091902), e: Bi-Sn-Te minerals (01091902), f: hessite (01091902), g: enargite (MUT-C1), and h: mixture of covellite and argentite (MUT-C1). *(a-h): in the south flank.

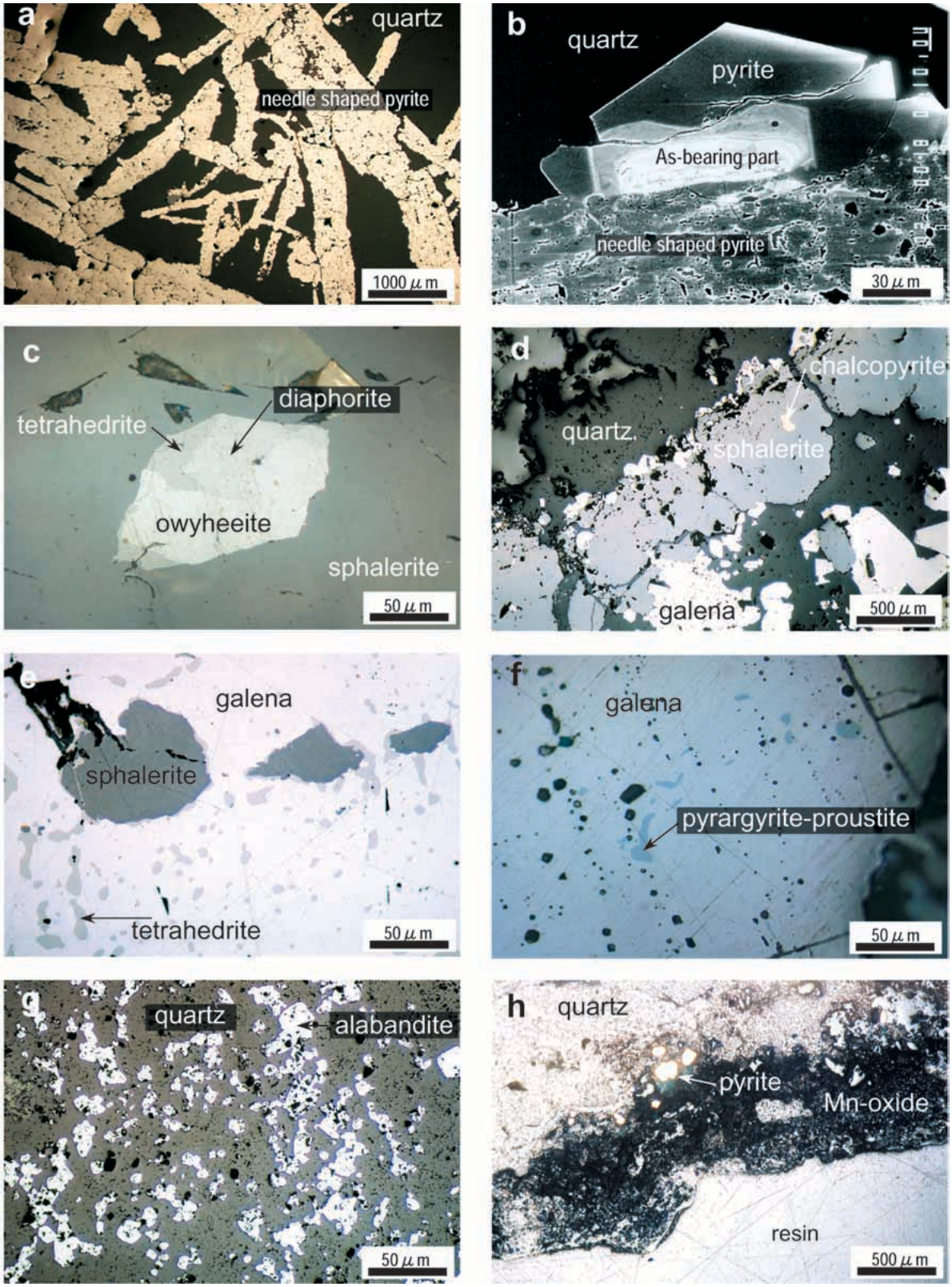

Fig. 7 Photomicrographs of ore minerals in the Mutnovskoe deposit. a: needle shaped of pyrite (0928-A), b: back scattered electron image of needle shaped pyrite with As concentration (0928-A), c: coexistence of diaphorite-owyheeite in sphalerite (0928-A), d: mineralized band of sphalerite (TM-98/4A), e: tetrahedrite emulsion in sphalerite (01091406), f: pyrargyrite emulsion in galena (0928-A), g: alabandite in quartz vein (K-017), and h: Mn-oxide layer (01091407). *(a-f, h): in the central flank; (g): in the south flank.

Table 3 Representative chemical composition of sphalerite.

Sample number	01091406	0928-Aβ	01091902	K-300	TM98-4A-1	MUT-S1	MUT-C1
Lab ID	509	14	335	126	440	69	48
Area*	C	C	S	S	S	S	S
Stage	I	I	I	I	I	I	I
Mineral	sph	sph	sph	sph	sph	sph	sph
Zn (wt%)	63.57	51.70	66.56	65.07	62.70	65.75	66.71
Fe	0.13	13.02	0.08	0.00	3.52	1.05	0.19
Cu	0.21	1.49	0.09	0.80	0.80	0.16	0.09
Mn	2.92	0.18	0.02	0.01	0.19	0.07	0.00
Cd	0.48	0.14	1.38	1.67	0.00	0.29	0.51
Sn	0.00	0.00	0.00	0.00	0.00	0.00	0.00
Ag	0.07	0.19	0.00	0.00	0.00	0.01	0.00
In	0.00	0.00	0.00	0.85	0.00	0.00	0.00
S	32.96	33.40	32.16	32.26	32.58	32.82	32.74
Total	100.34	100.12	100.29	100.66	99.79	100.16	100.23
Zn (atom%)	47.11	37.74	49.99	48.88	46.69	48.95	49.76
Fe	0.11	11.13	0.07	0.00	3.07	0.92	0.17
Cu	0.16	1.12	0.07	0.62	0.61	0.13	0.07
Mn	2.58	0.15	0.02	0.01	0.17	0.06	0.00
Cd	0.21	0.06	0.60	0.73	0.00	0.13	0.22
Sn	0.00	0.00	0.00	0.00	0.00	0.00	0.00
Ag	0.03	0.08	0.00	0.00	0.00	0.01	0.00
In	0.00	0.00	0.00	0.36	0.00	0.00	0.00
S	49.80	49.72	49.25	49.40	49.46	49.81	49.79
Total	100.00	100.00	100.00	100.00	100.00	100.00	100.00

Mineral abbreviation sph: sphalerite.
* N, C and S denote north, central and south flanks in Figure 2.

Table 4 Representative chemical composition of tetrahedrite-tennantite group minerals.

Sample number	TM-1	01091902	01091902	MUT-C1	MUT-C1	01091406
Lab ID	374	3	4	102	110	502
Area	C	S	S	S	S	C
Stage	II	I	I	I	I	I
Mineral	tet	gf	ten	ten	tet	tet
Cu(wt%)	38.25	41.65	40.72	43.56	39.01	34.87
Ag	0.83	5.37	1.08	0.15	1.03	4.71
Zn	7.44	1.70	6.48	4.17	1.55	5.16
Fe	0.36	2.09	0.74	2.41	2.27	0.35
Mn	0.29	0.24	0.89	1.15	2.87	0.80
As	9.31	8.56	9.39	20.21	6.39	1.55
Sb	18.11	2.99	14.79	1.02	21.24	28.23
Te	n.a.	12.68	0.00	0.10	0.00	n.a.
S	25.57	24.26	25.40	27.80	25.24	24.32
Total	100.15	99.54	99.48	100.56	99.60	99.98
Cu(atom %)	33.34	37.07	35.23	34.96	34.35	31.93
Ag	0.43	2.81	0.55	0.07	0.53	2.54
Zn	6.30	1.47	5.45	3.26	1.33	5.48
Fe	0.36	2.12	0.73	2.20	2.27	0.36
Mn	0.29	0.24	0.89	1.06	2.92	0.85
As	6.89	6.46	6.89	13.76	4.77	1.20
Sb	8.24	1.39	6.68	0.43	9.76	13.49
Te	n.a.	5.62	0.00	0.04	0.00	n.a.
S	44.17	42.81	43.57	44.22	44.06	44.14
Total	100.00	100.00	100.00	100.00	100.00	100.00

Mineral abbreviation gf: goldfieldite, ten: tennantite, tet: tetrahedrite.
n.a.: no analysis

II of Au-Ag quartz vein type ore from the north and the central flanks (Okrugin, 1995). A polymetallic vein also has higher Au grade (Table 1). Hessite [Ag_2Te] occurs with tennantite in the south flank (Fig. 6-f; Table 6). According to Okrugin (1995) and Lattanzi et al. (1995), calaverite [$AuTe_2$], petzite [Au_3AgTe_3] and sylvanite [$AuAgTe_4$] occur in stage I of the south flank.

4.2.6. Sn-Bi-minerals: Stannoidite [$Cu_5Sn(Te,Zn)_2S_8$] and tetradymite [Bi_2Te_2S] occur in stage I of the south flank (Table 7). Stannite [Cu_2SnFeS_4], canfieldite [$Ag_8(Sn,Ge)S_6$] and mawsonite [$Cu_{2+x}Sn_{1-x}FeS_4$] also occur in the south flank of the deposit (Lattanzi et al., 1995; Okrugin, 1995).

4.2.7. Ag-sulphosalts: Coexistence of diaphorite [$Pb_2Ag_3Sb_3S_8$] and owyheeite [$Pb_5Ag_2Sb_6S_{15}$] with 20–150 μm in size is observed in sphalerite of stage I of the central flank (Fig. 7-c). Pyrargyrite-proustite solid solution [$Ag_3(Sb,As)S_3$] occurs as exsolution in galena (Fig. 7-f) in the stage I of the central flank. EPMA analysis and microscopic observation indicate that pyrargyrite is the dominant species (Table 7). According to Lattanzi et al. (1995) and Okrugin (1995), argentite-acanthite [$Ag_2(Se,S)$], polybasite-pearceite [$(Ag,Cu)_3(As,Sb)_2S_{11}$], stephanite [Ag_5SbS_4] and sternbergite [$AgFe_2S_3$] also occur in the Mutnovskoe deposit.

4.2.8. Alabandite [MnS]: Alabandite forms a massive black band (1–3 cm in width) in quartz, rhodochrosite and calcite associated vein of stage III. The band is composed of aggregated allotriomorphic alabandite with size of 5–50 μm (Fig. 7-g). EPMA analysis indicates low Fe content (<0.1 wt%; Table 5).

4.2.9. Manganese oxide: Manganese oxide abundantly covers the surface of chiefly quartz vein type ores in some outcrops in the Mutnovskoe deposit (Fig. 4-e; Fig. 7-h). Mn-oxide could be a supergene genesis, identified as the last process of stage III.

5. Fluid Inclusions

5.1. Analytical method

Microthermometry was carried out on primary and pseudo-secondary fluid inclusions in quartz and sphalerite. Samples are 01091403 from the north flank, TM-98/4A from the central flank, 01091902, 01091903, MUT-C1, MUT-S1 and K-300A, from the south flank of the Mutnovskoe deposit. All of the selected host minerals belong to stage I with an exception

Table 5 Representative chemical composition of Fe-Cu-Mn minerals.

Sample number	0928Aβ	0928Aβ	01091902	K-300A	MUT-C1	MUT-C1	K-017
Lab ID	10	35	323	9	95	15	148
Area	C	C	S	S	S	S	S
Stage	I	I	I	I	I	I	III
Mineral	py	pyrr	py	cpy	cov*	eng	alb
(wt%)							
Fe	45.31	58.72	45.84	30.92	0.23	0.35	0.11
Cu	0.06	0.02	0.00	33.25	61.14	48.71	0.00
Mn	0.00	n.a.	0.00	0.00	0.00	0.00	63.23
Zn	0.00	n.a.	0.01	0.05	0.01	0.26	n.a.
Ag	0.00	0.00	0.00	0.00	5.67	0.03	0.00
Sb	0.01	0.00	0.01	n.a.	0.00	0.16	0.01
As	5.57	0.00	1.13	n.a.	0.00	18.69	0.04
S	48.67	40.05	53.09	34.85	32.63	32.01	37.07
Total	99.62	98.79	100.08	99.06	99.67	100.19	100.46
(atom %)							
Fe	33.74	45.69	32.93	25.58	0.20	0.31	0.09
Cu	0.04	0.01	0.00	24.17	47.23	37.83	0.00
Mn	0.00	n.a.	0.00	0.00	0.00	0.00	49.83
Zn	0.00	n.a.	0.00	0.04	0.01	0.19	n.a.
Ag	0.00	0.00	0.00	0.00	2.58	0.01	0.00
Sb	0.00	0.00	0.00	n.a.	0.00	0.07	0.01
As	3.09	0.00	0.61	n.a.	0.00	12.31	0.02
S	63.13	54.29	66.45	50.22	49.98	49.28	50.06
Total	100.00	100.00	100.00	100.00	100.00	100.00	100.00

Mineral abbreviation py: pyrite, pyrr: pyrrhotite, cpy: chalcopyrite, cov*: mixture of covellite and minor argentite, eng: enargite, alb: alabandite, n.a.: no analysis

Table 6 Representative chemical composition of telluride minerals.

Sample number	01091902	01091902	01091902	01091902
Lab ID	13	118	149	159
Area	S	S	S	S
Stage	I	I	I	I
Mineral	hes*	hes*	tdm	tdm
Ag (wt%)	61.07	57.81	1.64	3.24
Au	n.a.	0.31	0.00	0.00
Cu	1.84	2.04	n.a.	n.a.
Bi	n.a.	n.a.	55.41	56.26
Sb	0.09	0.01	0.60	0.43
As	0.01	0.00	0.04	0.09
Te	38.95	39.25	33.83	33.02
Se	n.a.	0.09	2.45	1.00
S	0.15	0.17	4.02	4.08
Total	102.12	99.67	97.99	98.11
Ag (atom %)	62.49	60.66	2.15	4.27
Au	n.a.	0.18	0.00	0.00
Cu	3.20	3.63	n.a.	n.a.
Bi	n.a.	n.a.	37.48	38.32
Sb	0.08	0.01	0.70	0.50
As	0.02	0.00	0.08	0.17
Te	33.69	34.82	37.47	36.84
Se	n.a.	0.12	4.39	1.80
S	0.52	0.59	17.74	18.11
Total	100.00	100.00	100.00	100.00

Mineral abbreviation *hes: mixture of hessite and minor tennantite, tdm: tetradymite. n.a.: no analysis.

of 01091403 from stage II. The data of homogenization temperature reported by MITI (2001) are referred about 01091403 for the north flank and 01091903 for the south flank. Low transparency of sphalerite and small size of fluid inclusions prevented to measure the homogenization temperature and salinity for some sphalerite specimens. Fluid inclusions with measurable size could not be found from TM-1. The rates of heating were 1-3˚C/min for homogenization and 0.1–0.3˚C/min for ice melting at the timing of phase change.

5.2. Microthermometry

Fluid inclusions are modally 15-20 μm in size, and take polygonal or irregular forms. Most of the fluid inclusions are liquid-vapor phase, and poly-phase fluid inclusions were not found except K-300A of vapor-rich inclusions.

In the north flank, the quartz sample of 01091403 from stage II shows homogenization temperature from 198 to 266˚C (av. 226˚C).

In the central flank, the quartz sample of TM-98/4A from stage I shows homogenization temperature from 202 to 266˚C (av. 235˚C) and salinity from 1.6 to 2.8 wt% NaCl equivalent (abbreviated hereafter to wt%) (av. 2.0 wt%).

In the south flank, the quartz sample of 01091902 from stage I shows homogenization temperature from 156 to 297˚C (av. 226˚C). The quartz sample of 01091903 from the stage I shows homogenization temperature from 232 to 282˚C (av. 248˚C). The quartz-sphalerite sample of

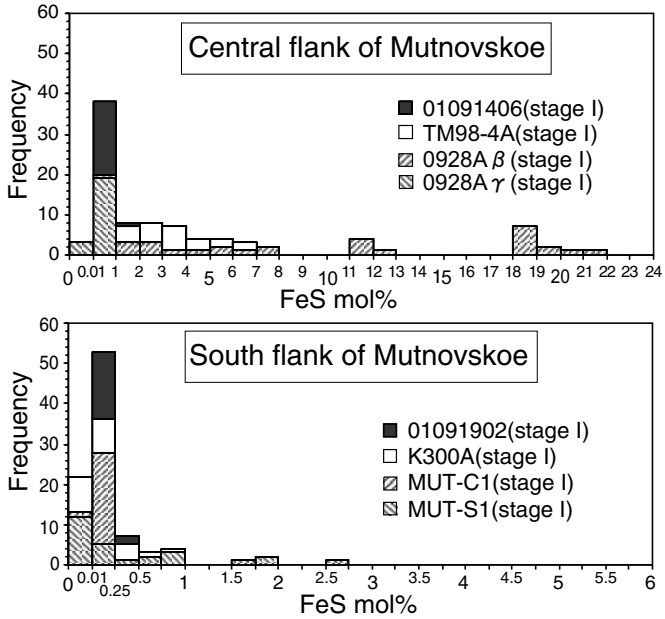

Fig. 8 FeS contents in sphalerite of the Mutnovskoe deposit. Note that detection limit of EPMA is 0.01 mol % FeS.

Table 7 Representative chemical composition of Ag-Pb-Sn minerals.

Sample number	0928Aβ	0928-Aα	0928-B	0928-B	01091902
Lab ID	50	128	124	123	10
Area	C	C	C	C	S
Stage	I	I	I	I	I
Mineral	gn	pyr	dia	owy	std
Ag (wt%)	0.16	60.07	23.92	5.84	0.07
Au	n.a.	0.97	0.00	0.00	n.a.
Pb	85.40	0.00	29.28	46.26	n.a.
Bi	0.00	n.a.	n.a.	n.a.	n.a.
Cu	0.00	0.05	0.17	0.33	39.48
Sn	n.a.	n.a.	n.a.	n.a.	17.90
Zn	n.a.	n.a.	n.a.	n.a.	4.15
Fe	0.05	n.a.	n.a.	n.a.	8.59
Mn	n.a.	n.a.	n.a.	n.a.	0.48
Sb	0.17	19.22	26.05	25.79	0.00
As	0.00	1.09	0.91	1.57	0.21
S	13.67	18.15	18.89	19.17	28.78
Te	n.a.	0.11	0.00	0.00	0.00
Se	n.a.	0.00	0.72	0.43	n.a.
Total	99.44	99.65	99.93	99.39	99.66
Ag (atom %)	0.17	42.77	18.64	4.84	0.03
Au	0.00	0.38	0.00	0.00	0.00
Pb	48.96	0.00	11.88	19.96	0.00
Bi	0.00	n.a.	n.a.	n.a.	n.a.
Cu	0.00	0.06	0.23	0.47	32.71
Sn	n.a.	n.a.	n.a.	n.a.	7.94
Zn	n.a.	n.a.	n.a.	n.a.	3.35
Fe	0.05	n.a.	n.a.	n.a.	8.10
Mn	n.a.	n.a.	n.a.	n.a.	0.46
Sb	0.17	12.12	17.98	18.93	0.00
As	0.00	1.12	1.02	1.88	0.15
S	50.65	43.48	49.50	53.44	47.26
Te	n.a.	0.07	0.00	0.00	0.00
Se	n.a.	0.00	0.76	0.48	0.00
Total	100.00	100.00	100.00	100.00	100.00

Mineral abbreviation gn: galena, pyr: pyrargyrite, dia: diaphorite, owy: owyheeite, std: stannoidite. n.a.: no analysis.

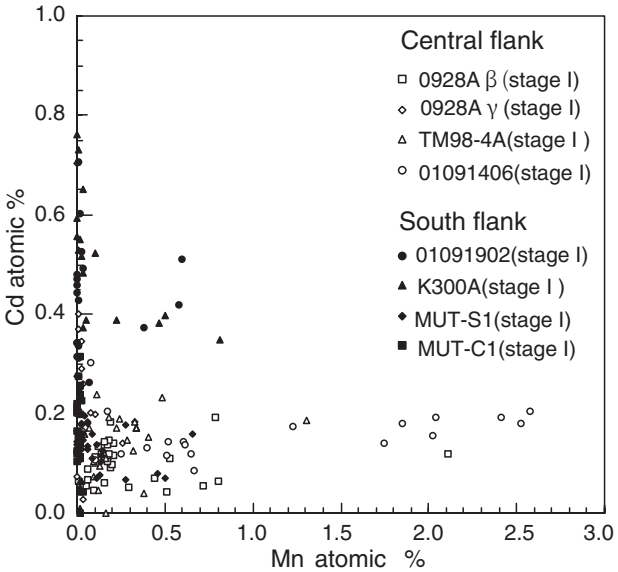

Fig. 9 Diagrams of Cd and Mn contents of sphalerite from the Mutnovskoe deposit.

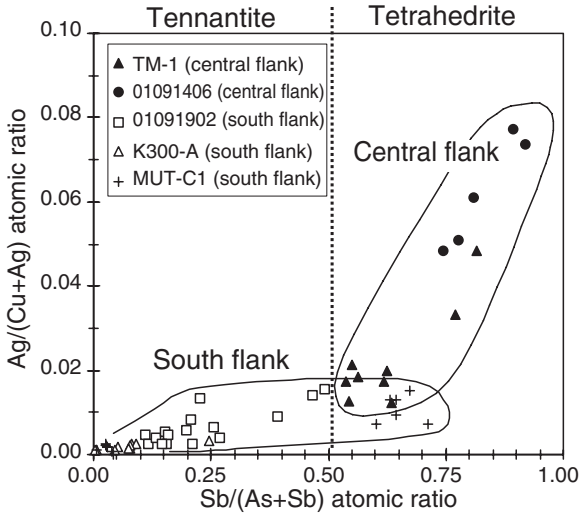

Fig. 10 Chemical compositions of tetrahedrite-tennantite group mineral in the Mutnovskoe deposit. Samples are from stage I except TM-1 from the stage II.

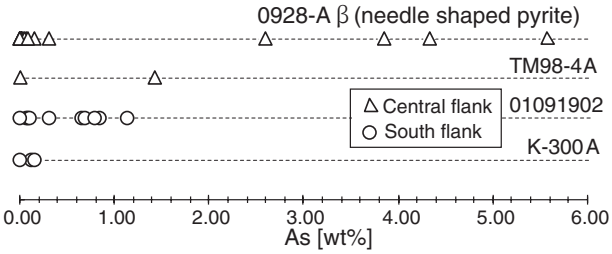

Fig. 11 Diagram of arsenic contents in pyrite of the stage I.

MUT-S1 from the stage I shows homogenization temperature from 198 to 273˚C (av. 234˚C) and salinity from 1.0 to 5.7 wt% (av. 2.7 wt%), which indicates higher salinity and lower temperature of primary inclusion in sphalerite than in quartz. The quartz - sphalerite sample of MUT-C1 from the stage I shows homogenization temperature from 192 to 236˚C (av. 219˚C) and salinity from 0.8 to 3.6 wt% (av. 3.2 wt%), which indicates higher salinity of primary inclusion in sphalerite than in quartz. The quartz sample of K-300A from the stage I shows homogenization temperature from 166 to 280˚C (av. 204˚C) and salinity from 0.8 to 3.3 wt% (av. 2.0 wt%) (Figs. 12 and 13).

Overview of the fluid inclusion study suggests higher salinity condition of sphalerite mineralization (2.2 - 5.7 wt%) than quartz mineralization (0.8 - 3.3 wt%).

6. Discussion

6.1. Physicochemical conditions of ore deposition

In this section, physicochemical conditions of ore deposition at the Mutnovskoe deposit are estimated on the basis of the homogenization temperature of fluid inclusions, sphalerite geothermometer (Barton and Toulmin, 1966), and univariant curve of ore mineral equilibria.

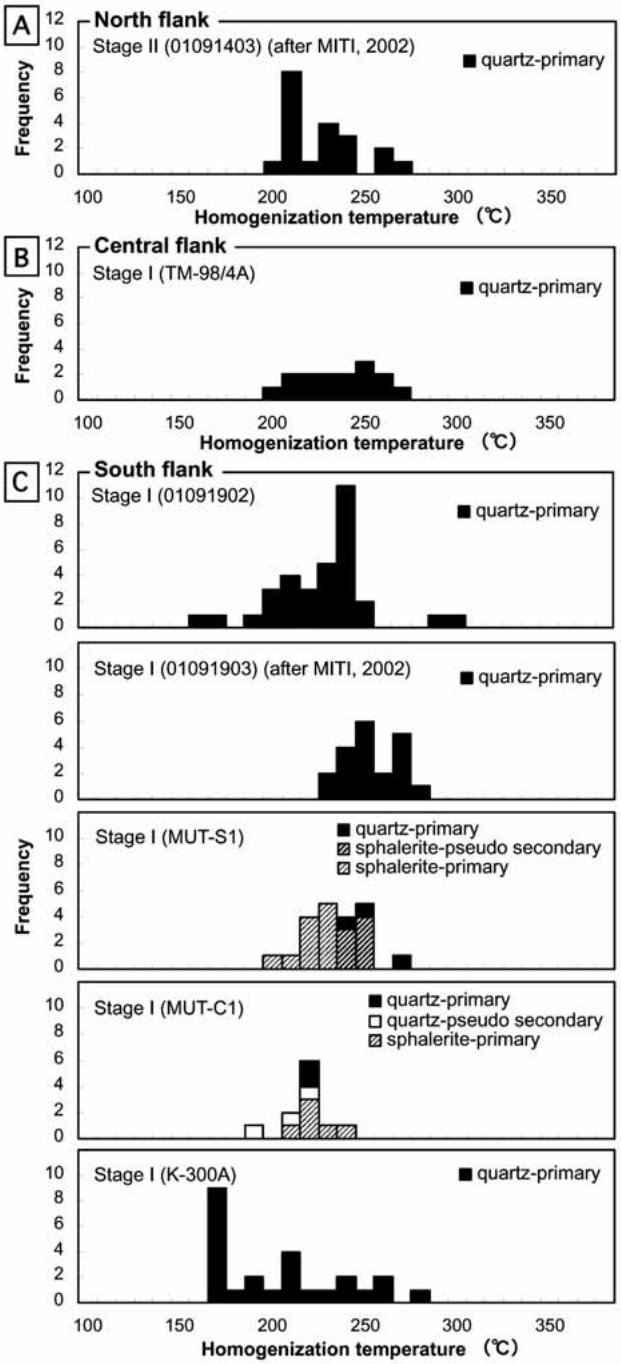

Fig. 12 Histograms of homogenization temperature of fluid inclusions at the Mutnovskoe deposit.

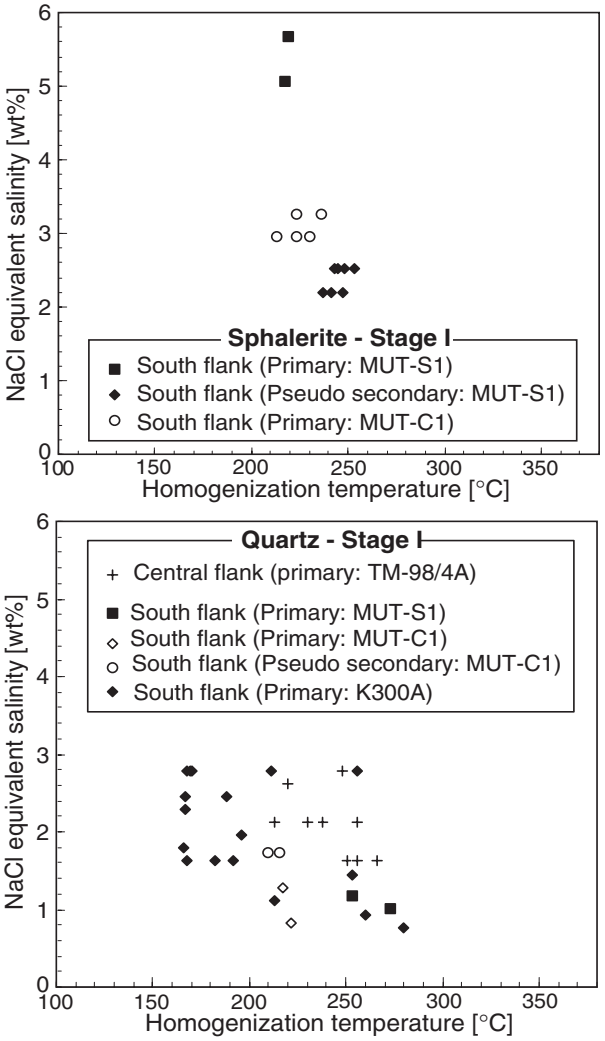

Fig. 13 Diagrams of salinity vs. homogenization temperature of fluid inclusions at the stage I for the Mutnovskoe deposit.

Estimated f_{S_2} - T conditions are illustrated in Figure 14. Formation depth of the Mutnovskoe deposit would be approximately below 500 m or below 1 km at most, on the basis of general erosion rate of 0.1–0.2 mm/year in island-arc (e.g. Hedenquist et al., 2000; Kaizuka, 1969). Thus homogenization temperatures are supposed to be identical to the trapping temperatures under 5–10 MPa in hydrostatic pressure. Exceptional data of low frequency (=1) were omitted from the histograms of homogenization temperature in Figure 12. Rounded approximate ranges of temperatures were applied: 210 to 260˚C (TM98/4A), 200 to 250˚C (01091902), 210 to 240˚C (MUT-C1) and 220 to 260˚C (MUT-S1). Enargite-tennantite curve borders upper limit of f_{S_2} conditions. The conditions of the pyrite-pyrrhotite coexistence and the estimate of [pH<5, T< 240˚C, with $H_2S_2(aq)$] (e.g. Murowchick, 1992) for marcasite precipitation were applied for 0928-A (Fig. 14).

A guideline defining the "high sulfidation" and the "low sulfidation" is understood to lie along the boundary of the enargite-tennantite curve in log f_{S_2}-T diagram, and enargite is used as a typical high-sulfidation mineral (Hedenquist et al., 1994; Sillitoe, 1989; e.g., Einaudi et al., 2003).

The polymetallic mineralization of stage I in the Mutnovskoe deposit would be in "low sulfidation state" (and/or "intermediate sulfidation" indicated e.g. by Einaudi et al., 2003). Specifically, log f_{S_2}-T diagram

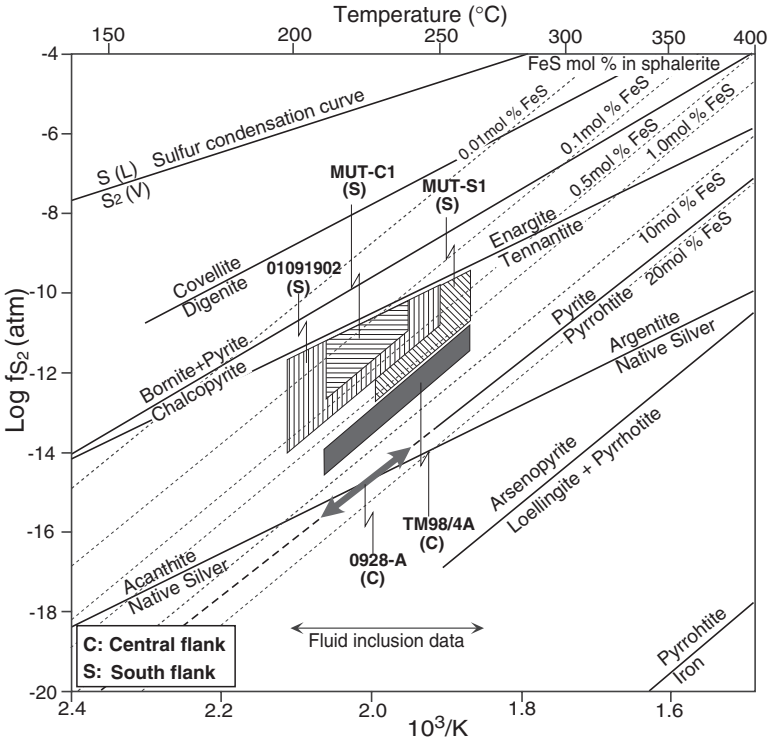

Fig. 14 Ore forming conditions estimated for the polymetallic vein (stage I) of the Mutnovskoe deposit. The univariant curves of argentite-native silver and sulfur condensation are quoted from Barton and Skinner (1967). The pyrite-pyrrhotite and bornite+pyrite - chalcopyrite curves are quoted from Scott and Barnes (1971). The enargite+tennantite curve is quoted from Craig and Barton (1973).

suggests that the south flank is in higher sulfidation state than the central flank. The typical Au-Ag quartz mineralization of the stage II could be in "low sulfidation" state based on the mineralogical association.

6.2. *Fractional crystallizations of tetrahedrite-tennantite and sphalerite*

Hackbarth and Petersen (1984) indicated the compositional field of natural tetrahedrite-tennantite solid solutions in Ag/(Cu+Ag)-Sb/(As+Sb) diagram, and summarized spatial composition zoning that tetrahedrite-tennantite samples from the central or deeper parts of a hydrothermal deposit are lower in Ag and Sb. Sack and Loucks (1985) summarized that tetrahedrite-tennantite solid solutions with intermediate $X_{Sb}/(X_{As}+X_{Sb})$ ratios have greater As/Sb ratios than the ore-forming solutions from which they precipitated. They suggested also that the tetrahedrite-tennantite solid solution evolves towards greater $X_{Sb}/(X_{As}+X_{Sb})$ ratios along the direction of flow of the ore-forming solutions, in which the tetrahedrite-tennantite is only As- and Sb-bearing ore phase. Their model is based on the changes of composition of the ore-forming solutions by crystallization of tetrahedrite-tennantite. At the polymetallic mineralization (stage I) of the Mutnovskoe deposit, the occurrence of the enargite as a trace As-bearing mineral could be negligible. Thus a district zoning (as defined, e.g. by Evans, 1997) of tetrahedrite with $X_{Sb}/(X_{As}+X_{Sb})$ = 0.74–0.91 in the central flank, and tennantite-tetrahedrite with $X_{Sb}/(X_{As}+X_{Sb})$=0.00–0.67 in the south flank (Fig. 10) would be a result of denudation of the spatial zoning. The spatial zoning would be due to the fractional crystallization from the evolving ore-forming solution as follows: (1) tennantite crystallization in a path of hydrothermal water relatively near to the heat source, (2) As depletion from the ore-forming solution, and (3) tetrahedrite crystallized in the path relatively far from the heat source.

According to the studies for sphalerite composition, the covalent elements are preferentially partitioned into sphalerite in order of Cd>Fe>Mn (Kubo et al., 1992) and Cd and Mn contents in sphalerite is commonly attribute to the chemical composition of ore-forming solution (Urabe, 1977; Nakayama, 1986). These researches suggest the possible Mn and Cd fractionation into sphalerite alike the tetrahedrite-tennantite solid solution discussed above. District zoning of Mn-rich sphalerite in the central flank, and Cd-rich sphalerite in the south flank (Fig. 9) would be a result of denudation of the spatial zoning. The spatial zoning would be due to the fractional crystallization from the evolving ore-forming solution as follows: (1) Cd-rich sphalerite crystallization in a path of hydrothermal water relatively near to the heat source, (2) Cd depletion from the ore-forming solution, and (3) Mn-rich sphalerite crystallized in the path relatively far from the heat source.

6.3. *Future subject*

Non-Gaussian distribution of homogenization temperatures is recognized, and some higher temperature inclusions show low salinity for a polymetallic ore of K-300A from the south flank (Figs. 12 and 13). Quartz part of this ore hosts brecciated sphalerite. These observations indicate a possibility of boiling phenomenon at the mineralization temperature around 170˚C, which will be clarified by a future study.

K-Ar ages of the Pleistocene volcanics from 0.80± 0.04 to 0.63±0.03 Ma (Sheimovich and Karpenko, 1996) should be reviewed from a point of view of the overprint by hydrothermal activities, as the mineralization age of 0.7±0.1 Ma is shown for the stage II.

A hypothesis is inferred that the magmatic heat source differentiated the deposit into the central and the south

flanks by their path distances of the flow of hydrothermal fluid. This hypothesis is based on following considerations: (1) higher sulfidation state in the south flank than in the central flank on the f_{S_2}-T diagram (Fig. 14), (2) spatial zoning and fractional crystallizations of tetrahedrite-tennantite solid solution and Cd- and Mn-rich sphalerite, and (3) modally higher Pb-Zn contents of ores in the south flank than in the central flank (Fig. 3), by using representative samples of the Mutnovskoe deposit. For the sake of this discussion, a question remains why temperature gradient is not recognized between the central and the south flanks (Fig. 12). And it will be needed to clarify the details of ore-forming condition in the north flank for future subject.

7. Conclusions

The Mutnovskoe deposit is divided into the north, the central and the south flanks based on the vein distributions and the mineral parageneses. Mineralization stages are stage I (polymetallic vein) mainly in the central and the south flanks, the stage II (Au-Ag quartz vein) mainly in the north and the central flank, and the stage III (Mn-sulfide and Mn-Ca-carbonate vein) in the whole area of the deposit. The K-Ar ages are 1.3±0.1 Ma for the stage I, and 0.7±0.1 Ma for the stage II.

The mineralized veins show zoning distributions of modally higher Pb-Zn contents in order of the south flank > the central flank > the north flank. Zoning of the mineral paragenesis of tennantite and Cd-rich sphalerite for the south flank and tetrahedrite and Mn-rich sphalerite for the central flank is observed in the stage I, which would be due to the fractional crystallizations of ore-forming fluid.

Fluid inclusion study indicates the ore forming temperature of 200–260˚C (av. 230˚C), representing the stages I and II including the north, the central and the south flanks. NaCl equivalent salinity is 2.2–5.7 wt% for sphalerite mineralization, while 0.8–3.3 wt% for quartz mineralization. FeS contents of sphalerite are about 0–22 mol % for the central flank, while 0 - 1 mol % for the south flank.

Physicochemical estimation indicates the depositional condition of low sulfidation state for the whole Mutnovskoe deposit. Although there is not much difference of ore-forming temperatures, the sulfidation state of the stage I is relatively higher for the south flank than the central flank.

Acknowledgments: The research was partly supported by the Sasagawa Scientific Research Grant from The Japan Science Society. A part of ore samples were contributed from Ministry of International Trade and Industry, and we would like to express our sincere gratitude to Kenichi Kurihara of MITI as the coordinator. We thank to Hideo Kudo and Takashi Kageyama of Dowa Mining Co., Ltd. for the grade analysis of ores. We also extend our thanks to Fumiaki Takeda of Hokkaido University, Elena D. Andreyeva and Ksenia O. Sheshcanova of Kamchatka University for their helpful support at the field work. We are grateful to Anna M. Okrugina, Takamura Tsuchiya, Osamu Fujikawa, Takeyuki Ogata, Shunsuke Sakai, Mega F. Rosana and Srinivas Sarella for their helpful advice concerning this study. We are grateful to David H. Green of Australian National University for his checking the English manuscript. Suggestions from two anonymous *Resource Geology* reviewers and advice from Kohei Sato of *Resource Geology* editor improved this paper significantly.

References

Barton, P. B., Jr. and Toulmin, P. III (1966) Phase relations involving sphalerite in the Fe-Zn-S system. Econ. Geol., 611, 815–849.

Barton, P. B., Jr. and Skinner, B. J. (1967) Sulfide mineral stabilities. *in* Barnes, H. L. (ed.) Geochemistry of Hydrothermal Ore Deposits. 236–333, Holt, Rinehart, and Winston, New York.

Craig, J. R. and Barton, P. B., Jr. (1973) Thermochemical approximations for sulfosalts. Econ. Geol., 68, 493–506.

Einaudi, M. T., Hedenquist, J. W. and Inan, E. (2003) Sulfidation state of hydrothermal fluids. The porphyry-epithermal transition and beyond. *in* Simmons, S. F. and Graham, I. J. (eds.) Volcanic, Geothermal and Ore-forming Fluids, Rulers and Witnesses of Processes within the Earth. Soc. Econ. Geol. and Geochem. Soc., Spec. Publ., 10, 285–313.

Evans, A. M. (1997) An Introduction to Economic Geology and Its Environmental Impact. Blackwell Science, Inc., 364p.

Fedotov, S. A. (1991) On the mechanism of volcanic activity in Kamchatka, Kuril-Kamchatka arc and in similar structures. *in* Fedotov, S. A. and Masurenkov, Yu. P. (eds.) Active Volcanoes of Kamchatka. Moscow, Nauka, 1, 30–35.

Hackbarth, C. J. and Petersen, U. (1984) A fractional crystallization model for the deposition of argentian tetrahedrite. Econ. Geol. 79, 448–460.

Hedenquist, J. W., Matsuhisa, Y., Izawa, E., White, N. C., Giggenbach, W. F. and Aoki, M. (1994) Mineralogy, geochemistry, and origin of high sulfidation Cu-Au mineralization in the Nansatsu district, Japan. Econ. Geol., 89, 1–30.

Hedenquist, J. W., Izawa, E., Arribas, A. and White, N. C. (1996) Epithermal Gold Deposits: Styles, Characteristics, and Exploration. Soc. Resource Geol. Spec. Publ., 1, 17p.

Hedenquist, J. W., Arribas, A. Jr. and Gonzalez-Urien, E. (2000) Exploration for epithermal gold deposits. Rev. Econ. Geol., 13, 245–277.

Kaizuka, S. (1969) Changing landforms - Under tectonic movement, sea level change and climatic change. Kagaku, 39, 11–19 (in Japanese).

Kirsanov, I. T. and Melekestsev, I. V. (1991) Gorely Volcano. *in* Fedotov, S. A. and Masurenkov, Yu. P. (eds.) Active Volcanoes of Kamchatka. Moscow, Nauka, 2, 27, 314–315.

Kubo, T., Nakato, T. and Uchida, E. (1992) An experimental study on partitioning of Zn, Fe, Mn and Cd between sphalerite and aqueous chloride solution. Resource Geol., 42, 301–309.

Kutina, J. (1955) Genetische Diskussion der Makrotexturen bei der geochemische Untersuchung des Adalbert-Hauptganges in Pribram. Chemie Erde, 17, 241–323 (in Germany) .

Lattanzi, P., Okrugin, V. M., Corsini, A., Okrugina, A.,

Tchubarov, V. and Livi, S. (1995) Base and precious metal mineralization in the Mutnovsky area, Kamchatka, Russia. Soc. Econ. Geol. News Lett., 20, 5–9.

Leonov, V. (2000) Regional structural positions of high temperature hydrothermal systems of Kamchatka. *in* Proc. World Geothermal Congress Kyushu - Tohoku, Japan, 1377–1382.

Liessman, W. and Okrugin, V. M. (1994) Zur Lagerstaettenkunde der Halbinsel Kamchatka/Russland. Erzmetall, 47, 6, 376–393 (in Germany).

Masurenkov, Yu. P. (1991) Tectonic position and general history and evolution of Eastern Kamchatka Volcanoes. *in* Fedotov, S. A. and Masurenkov, Yu. P. (eds.) Active Volcanoes of Kamchatka. Moscow, Nauka, 1, 21, 14–15.

Melekestsev, I. V., Braitseva, O. A. and Ponomareva, V. V. (1987) Dynamics of Mutnovsky and Gorely volcanoes activity during the Holocene and volcanic hazard in adjacent areas (based on the data of tephrochronology). Volcanol. Seismol., 3, 3–18 (in Russian).

Ministry of International Trade and Industry (2001) Far East Area. Researching Report of Satellite Image Analysis on 2000, Metal Mining Agency of Japan, 45p.

Ministry of International Trade and Industry (2002) Far East Area. Researching Report of Satellite Image Analysis on 2001, Metal Mining Agency of Japan, 62p.

Murowchick, B. J. (1992) Marcasite inversion and the petrographic determination of pyrite ancestry. Econ. Geol., 87, 1141–1152.

Nakamura, T. (1988) Concept of mineral paragenesis and criteria for distinguishing mineralization stages in ore veins. *in* Sugaki, A. (ed.) Ore Microscope and Ore Texture. 445-455, Terra Scientific Publishing, Co., Tokyo (in Japanese).

Nakayama, E. (1986) Chemical composition of sphalerite from the Nebazawa gold-silver mine, Gunma prefecture, and its bearing on the evolution of ore fluid. Mining Geol., 36, 523–533.

Nally, M. (2003) The Asacha and Rodnikovoe gold project in Kamchatka, Russia. Trans-Siberian Gold Limited (UK). *in* Proc. of Asian Update on Mineral Exploration and Development, SMEDG - AIG Symp., Session 2-2.

Okrugin, V. M. (1995) Part 1 Mutnovsky geothermal field: Mutnovsky Hydrothermal Field Uzon-Geyser Depression. *in* Chudaev (ed.) Post-Session Field Trip to Kamchatka. 8th Intern. Symp. Water-Rock Interaction, Vladivostok, Russia, 1–29.

Okrugin, V. M., Stefanov, J. M., Shuvalov, R. A. and Stepanov, I. I. (1994a) On ecological-geochemical monitoring in Kamchatka (the Mutnovsky-Asachinsky ore region). Mineral. Mag., Goldschmidt Conf., Edinburgh, 58A, 671.

Okrugin, V. M., Okrugina A. M., Polushin, S. V. and Chubarov, V. N. (1994b) Sulphides of contemporary land and submarine hydrothermal systems of Kamchatka. Mineral. Mag., Goldschmidt Conf., Edinburgh, 58A, 670.

Okrugin, V. M., Zelenskii, M. E., Marynova, V. K., Okrugina, A. M., Senyukov, S. L. and Sergeeva, S. V. (2001) Last news about volcanic activity in Kamchatka Peninsula: Mutnovsky and Gorely volcanoes especially. *in* Proc. 2nd Intern. Workshop on Global Change: Connection to the Arctic, 2001. 1, 146–163, Research Center for North Eurasia and North Pacific Regions, Hokkaido Univ.

Patoka, M. G., Litovinov, A. F. and Petrenko, I. D. (1998) Kamchatka - A new gold bearing province of Russia. *in* Proc. on Russian-Japanese Field Seminar - Mineralization in Arc Volcanic-hydrothermal Systems (Kamchatka, Kuril and Japanese Isles). 72–75, Petropavlovsk-Kamchatsky, Russia.

Petrenko, I. D. (1998a) Structural position of the gold-silver deposit of Southern Kamchatka ore field. *in* Leonov, V. (ed.) Present Hydrothermal Systems and Epithermal Gold-silver Deposits of Kamchatka. Field Excursion Guide, Institute of Volcanology, Far East division, Russian Academy of Sciences, 65–67.

Petrenko, I. D. (1998b) Mutnovskoe deposit. *in* Leonov, V. (ed.) Present Hydrothermal Systems and Epithermal Gold-silver Deposits of Kamchatka. Field Excursion Guide, Institute of Volcanology, Far East division, Russian Academy of Sciences, 73–78.

Petrenko, I. D. (1999) Gold-Silver Formation of Kamchatka. VSEGEI, S-Petersburg, 115p.

Petrenko, I. D. and Bolshakov, N. M. (1995) Structural position and age of Au-Ag mineralization of southern Kamchatka (Mutnovskoe ore field). Geol. Pacific Ocean, 5, 100–111.

Petrenko, I. D. and Ozornin, P. A. (1998) Rodnikovoe deposit. *in* Leonov, V. (ed.) Present Hydrothermal Systems and Epithermal Gold-silver Deposits of Kamchatka. Field Excursion Guide, Institute of Volcanology, Far East Division, Russian Academy of Sciences, 67–72.

Sack, R. O. and Loucks, R. R. (1985) Thermodynamic properties of tetrahedrite-tennantites: constraints on the interdependencies of the Ag-Cu, Fe-Zn, Cu-Fe, and As-Sb exchange reactions. Amer. Mineral., 70, 1270–1289.

Scott, S. D. and Barnes, H. L. (1971) Sphalerite geothermometry and geobarometry. Econ. Geol., 66, 653–669.

Sheimovich, V. S. and Karpenko, M. I. (1996) K-Ar age of volcanism in South Kamchatka. Volcanol. Seismol., 18, 231–236.

Sillitoe, R. H. (1989) Gold deposits in western Pacific island arcs: The magmatic connection. Econ. Geol. Monogr. 6, 274–291.

Takahashi, R., Matsueda, H. and Okrugin, V. M. (2001) Epithermal gold and silver mineralization at the Rodnikovoe deposit related to the hydrothermal activity in the Mutnovsko-Asachinskaya geothermal area, Southern Kamchatka, Russia. *in* Proc. Intern. Symp. on Gold and Hydrothermal Systems, Fukuoka, Japan, 51–56.

Takahashi, R., Matsueda, H. and Okrugin, V. M. (2002) Hydrothermal gold mineralization at the Rodnikovoe Deposit in South Kamchatka, Russia. Resource Geol., 52, 359–369.

Trans-Siberian Gold PLC (2004) Asacha Gold Project-Environmental Assessment. MDS Mining & Environmental Services Ltd., UK, 137p.

Urabe, T. (1977) Partition of cadmium and manganese between coexisting sphalerite and galena from some Japanese epithermal deposits. Mineral. Deposita, 12, 319–330.

Vasilevsky, M. M., Stefanov, Y. M., Shiroky, B. I., Kutyev, F. S. and Okrugin, V. M. (1977a) Metallogeny of Kamchatka upper structural story and the problem of ore specialization of folded regions tectonic-magmatic evolution. *in* Vasilevsky, M. M. (ed.) Forecasting Estimation of Ore Content of Volcanogenic Formation. 14–60, Nedra, Moscow.

Vasilevsky, M. M., Zimin, V. M. and Okrugin, V. M. (1977b) Volcanogenic ore centers of the southeastern Kamchatka. *in* Vasilevsky, M. M. (ed.) Inferred Reserves of Ore-bearing Volcanic Formation. 122–128, Nedra, Moscow.

Vlasov, G. M. (1967) Kamchatka, Kuril, and Komandorskiye Islands - Geological description. *in* Geology of the USSR. 1–827, Nedra, Moscow.

Zonenshain, L. P., Kuzmin, M. I. and Natapov, L. M. (1990) A plate tectonic synthesis. Amer. Geophys. Union, Geodynamics Series, 21, 1–242.

(Editorial handling: Kohei SATO)